Surface Science 615 (2013) 57–64

Contents lists available at SciVerse ScienceDirect

Surface Science

journal homepage: www.elsevier.com/locate/susc

Oxygen subsurface adsorption on the Cu(110)-$c(6 \times 2)$ surface

Liang Li, Guangwen Zhou *

Department of Mechanical Engineering & Multidisciplinary Program in Materials Science and Engineering, State University of New York at Binghamton, NY 13902, United States

ARTICLE INFO

Article history:
Received 1 February 2013
Accepted 9 April 2013
Available online 15 April 2013

Keywords:
Oxygen chemisorption and reconstruction
Density functional calculations
Cu(110)
Oxidation

ABSTRACT

To understand the initial steps of the oxidation of Cu(110), we applied density functional theory (DFT) calculations to study oxygen subsurface adsorption at the Cu(110)-$c(6 \times 2)$ reconstructed surface by increasing oxygen coverage. A transition from oxygen octahedral occupancy to tetrahedral preference occurs when the coverage reaches 1 monolayer, which may signal the onset of bulk oxidation that initially forms highly distorted Cu – O tetrahedrons by comparing the bond lengths and angles of the resulting Cu – O tetrahedron with the bulk Cu_2O structure. These results suggest that a critical oxygen coverage is required for such a crossover from the oxygen chemisorption to bulk oxide formation. A comparison with the oxygen subsurface adsorption at Cu(100) suggests that the Cu(110) surface has a larger tendency to form Cu – O tetrahedrons.

1. Introduction

The interaction of oxygen with metals plays a critical role for a wide set of technological applications including chemical catalysis [1–3], corrosion [4,5], high temperature oxidation [6,7], gas sensing [8–10] and thin film processing [11–13]. Oxygen has been studied on many metal surfaces and in many cases and it has been shown that oxygen adsorption takes place with a significant surface restructuring which precedes the formation of a passivating oxide film. However, while many questions of the structure and kinetics of oxygen chemisorption are now answered, there is still a lack of a fundamental understanding of the crossover between oxygen surface chemisorption and bulk oxide formation. While it is widely assumed that the oxygen atoms are embedded into subsurface regions when the surface reconstruction is terminated at a high oxygen coverage whereby initializing the oxide formation [14–20], the atomic details of oxygen-adsorption induced transformation of the metal crystal lattice into its oxide are not elucidated.

Oxygen on copper has provided a model chemisorption system which has been subjected to a large number of studies. Particularly, the oxygen chemisorption on Cu(110), the most open of the low-index surfaces, is among the best studied systems, involving oxygen adsorption, interdiffusion of Cu and O, and various restructuring phases [21–32]. A consensus has been established that the Cu(110)-(2×1)-O phase induced by oxygen exposure appears to be "added rows" of Cu – O-Cu chains growing preferentially along the [001] direction, with the saturation oxygen coverage $\theta = 0.5$ [23,24]. Continuous oxygen adsorption causes further surface reconstruction into a Cu(110)-$c(6 \times 2)$ structure [21,22]. By using scanning tunneling microscopy (STM) and surface X-ray-diffraction investigations, Feidenhans'l et al. first derived the structural model for the $c(6 \times 2)$ reconstruction with a saturated oxygen coverage $\theta = 2/3$ [26]. In addition to the experimental observations, significant theoretical studies have also been performed, particularly on the Cu(110)-(2×1)-O reconstruction. Using density functional theory (DFT) calculations, Frechard et al. studied different atomic oxygen adsorption scenarios on the Cu(110) surface at low oxygen coverage. They found that the added-row configuration is the most stable phase among various structures because the missing surface Cu atoms can effectively release the surface tension [28]. Their results are supported by Liem et al., who also concluded that the added-row (2×1)-O reconstruction yields the lowest system energy at half oxygen coverage [29]. However, the study on the Cu(110)-$c(6 \times 2)$ reconstruction has been significantly fewer, and it remains unclear that how this structure evolves under further increased oxygen coverages.

In FCC (face-centered cubic) Cu lattice, two types of interstitial sites, i.e., octahedral and tetrahedral sites, are available for possible subsurface oxygen occupancy. It has been shown that octahedral sites are energetically more favorable than tetrahedral sites for oxygen subsurface adsorption at Cu(100) surface [14–17] though no similar studies have been yet performed on the Cu(110)-$c(6 \times 2)$ surface. However, for bulk Cu_2O structure oxygen atoms reside the tetrahedral sites in the Cu lattice. Therefore, transformation from the octahedral preference to the tetrahedral preference represents a crucial step in the onset of the bulk oxide formation. Yet, the atomic mechanism for such a transformation has not been established due largely to the lack of experimental approaches with the sufficient detectability to resolve the oxygen adsorption at the two subsurface sites. The goal of this work is to employ DFT calculations to investigate the structural evolution of the Cu(110)-$c(6 \times 2)$ reconstructed surface under high oxygen coverages and explore energetically favorable sites for oxygen subsurface adsorption, which will provide insight into the underlying mechanisms of the transition from the $c(6 \times 2)$ chemisorption to bulk Cu_2O formation.

* Corresponding author. Tel.: +1 6077775084; fax: +1 6077774620.
E-mail address: gzhou@binghamton.edu (G. Zhou).

0039-6028/$ – see front matter © 2013 Elsevier B.V. All rights reserved.
http://dx.doi.org/10.1016/j.susc.2013.04.005

2. Computational methodology

The DFT calculations are performed using the Vienna ab-initio simulation package (VASP) [33–36] with the PW91 generalized gradient approximation (GGA) [37] and projector augmented wave (PAW) potentials [38,39]. Our test calculation confirmed that a cutoff energy of 380 eV is sufficient to give a well converged adsorption energy [40]. The Cu surface is modeled by a periodically repeated slab consisting of five layers with the bottom layer fixed while the other layers are free to relax. Successive slabs are separated by a vacuum region of 11 Å. The Brillouin zone sampling is based on the Monkhorst–Pack technique [41]. We carried out a convergence test of the K-points mesh by comparing the total energy difference of a pure $c(6 \times 2)$ reconstructed slab using $4 \times 2 \times 1$ and $8 \times 4 \times 1$ meshes. A test with $8 \times 4 \times 1$ mesh gives a total energy difference of 0.025 eV, suggesting that sufficient convergence is reached using a $4 \times 2 \times 1$ mesh for the Cu(110) $c(6 \times 2)$ unit cell. Electron smearing is carried out following the Methfessel–Paxton technique [42] with $N = 1$ and $\sigma = 0.2$. The relaxation of the ionic positions into the ground state geometry is performed either with a conjugate gradient algorithm or a quasi-Newton scheme. To ensure the convergence, we also relax the clean five-layer Cu(110) slab and compare the interlayer spacings of the top few layers with the previously reported computational values. The height of each layer is defined as the average height of all atoms in that layer, and the interlayer separation is measured by the percent changes relative to the bulk value. Our results show that after structural relaxation, the spacing change between the first and second Cu layers is −10.3% and the second and third layers is 3.0%, which are in good agreement with the previously reported values of −10.0% and 3.0% by Duan et al. [31].

In this study, the oxygen adsorption energies and surface morphology changes under different oxygen coverages are investigated in a sequential manner. That is the most stable configuration identified from the low oxygen coverage is subsequently used as the reference system to determine the most stable configuration resulting from a

Table 1
The adsorption energies of the subsurface oxygen atom at the oxygen coverage $\theta = 3/4$ (8 on-surface and 1 subsurface oxygen atoms). The abbreviations for the adsorption sites are defined in Fig. 1.

Adsorption site	Adsorption energy E_{ads}/eV
Op1	−0.90
O1	−0.61
O3	−0.71
T1	−0.59
T2	−0.50

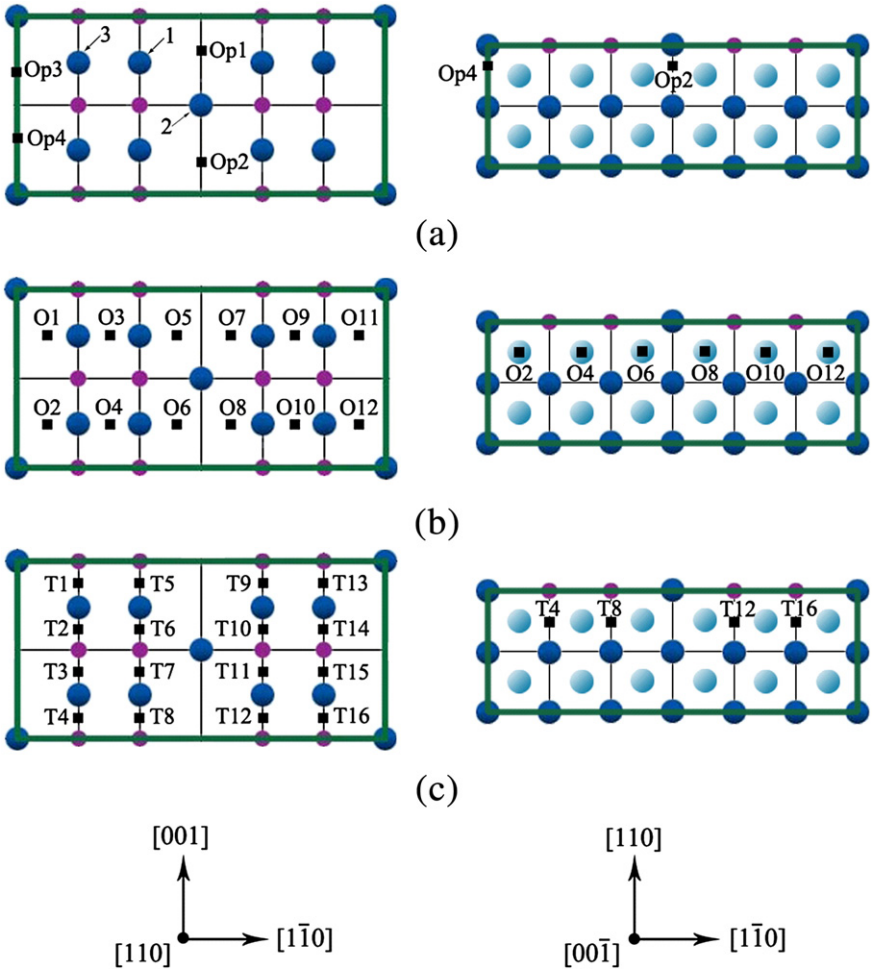

Fig. 1. Structural model of the Cu(110)-$c(6 \times 2)$ unit cell and the approximate locations of the subsurface sites for possible oxygen occupancy, left: top view along the [110] projection, right: side view along the $[00\bar{1}]$ projection (note that a five-layer slab is used). (a) 4 open (Op) sites (in the side view, the visualization of Op1 and Op3 is blocked by Op2 and Op4, respectively). Details of the Cu atoms labeled by 1, 2 and 3 in the top view can be found in the text. (b) 12 octahedral (O) sites (the view of O1. O3, O5, O7, and O11 is blocked in the side view). (c) 16 tetrahedral (T) sites (similarly, the visualization of the remaining tetrahedral sites is invisible in the side view).

higher oxygen coverage. The oxygen adsorption energy E_{ads} is calculated using the equation

$$E_{ads} = \frac{1}{N_O}\left(E^{tot}_{O/Cu} - E_{ref} - \frac{N_O}{2}E_{O_2}\right),$$

where $E^{tot}_{O/Cu}$ is the total energy of the Cu – O system, and E_{ref} is the energy of the structure that we use as a reference to compare the relative stability, and more specifically, it is the total energy of the most stable configuration with one less subsurface oxygen atom compared with the system under study. E_{O_2} is the energy of an isolated oxygen molecule and N_O is the number of oxygen atoms newly adsorbed into the system, which is equal to 1 throughout this work for sequentially increasing the oxygen coverage. The atomic structures are all visualized using the XCrySDen package [43]. The calculations of molecular and atomic oxygen are spin-polarized, and the binding energy of an oxygen molecule is calculated as 6.30 eV while the experimental value is 5.10 eV [44]. The GGA/PW91 error for the binding energy for O_2 is large as note before, and our value agrees with previous results [29,45,46].

Table 2
The adsorption energies of the subsurface oxygen atoms at the oxygen coverage $\theta = 5/6$ (8 on-surface and two subsurface oxygen atoms with the Op1 configuration).

Adsorption site	Adsorption energy E_{ads}/eV	Stabilized site
Op2	−0.49	
Op3	−0.84	
Op4	−0.79	
O1	−0.58	
O2	−0.57	
O3	−0.61	
O4	−0.49	
O5	−0.59	T6
O6	−0.61	
T1	−0.47	
T2	−0.44	
T3	−0.34	
T4	−0.50	
T5	−0.61	O3
T6	−0.59	
T7	−0.36	
T8	−0.61	O6

3. Computational results

Shown in Fig. 1(a) is a structural model of the Cu(110)-$c(6 \times 2)$ reconstructed surface with the saturated oxygen coverage of $\theta = 2/3$. The coverage is defined as the ratio of the number of oxygen atoms over the number of Cu atoms in the corresponding clean surface. For the Cu(110)-$c(6 \times 2)$ reconstruction, there are two adjacent [001]-oriented Cu – O – Cu rows in every three [110]-(1×1) lattice spacings. On every third [001] rows that do not contain Cu – O – Cu chains, every two [001] (1×1) lattice spacings are filled with alternate Cu atoms and vacancies, and these Cu atoms are bonded with the O atoms in the vicinal Cu – O – Cu chains [26]. Such a reconstruction has a large unit cell which gives rise to a number of distinct subsurface adsorption sites for oxygen atoms: four open sites (Op) which are located along the open [001] Cu rows (Fig. 1.(a)), 12 octahedral sites (Fig. 1.(b)), and 16 tetrahedral sites (Fig. 1.(c)). In this work, the oxygen coverage is increased gradually from $\theta = 2/3$ to $\theta = 1$, and the most energetically stable configuration is determined for each oxygen coverage.

We first check if oxygen atoms can still be embedded into the system via on-surface adsorption for the Cu(110)-$c(6 \times 2)$ reconstruction. Oxygen adsorption may occur on top of on-surface Cu atoms or short-bridge sites between Cu atoms along the [110] direction (note that the short-bridge sites between O atoms are obviously not favorable sites for O occupancy due to strong repulsion from the

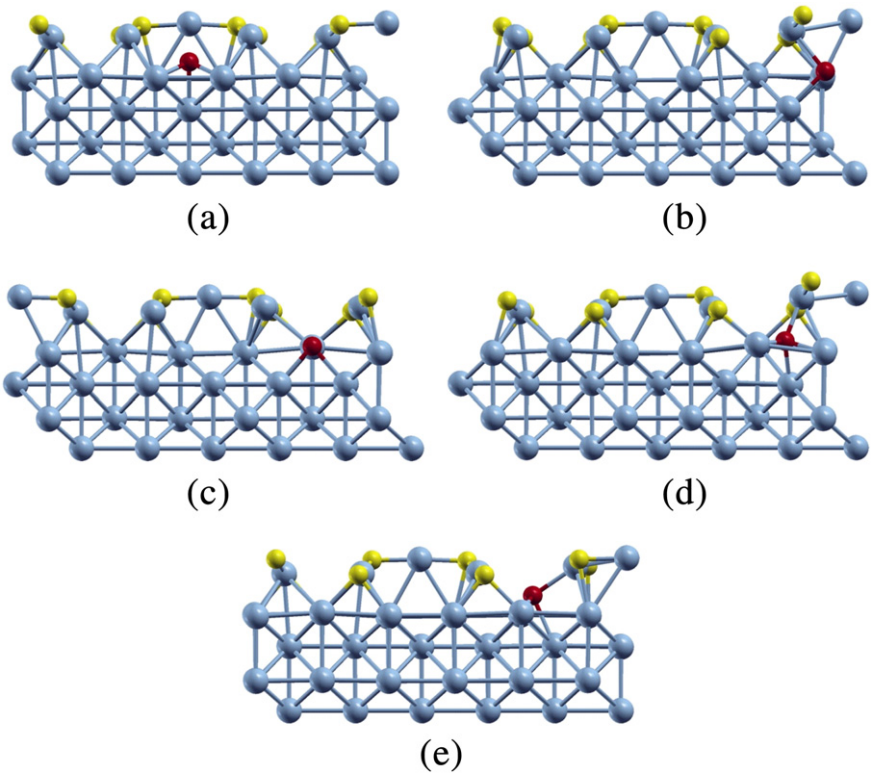

Fig. 2. Relaxed structures of the $c(6 \times 2)$ cell at an oxygen coverage of $\theta = 3/4$ with oxygen atoms adsorbed at various subsurface sites: (a) Op1, (b) O1, (c) O3, (d) T1, and (e) T2. Cu atoms are depicted by blue balls, on-surface oxygen atoms by yellow balls. Red balls represent the newly adsorbed subsurface oxygen atoms.

adjacent O atoms, see Fig. 1(a)). For the oxygen adsorption atop on-surface Cu atoms, the first layer of the supercell contains 10 Cu atoms, but there are only two nonequivalent sites (labeled 1 and 2 in Fig. 1(a)) due to the symmetries of the supercell. After structural relaxation, the oxygen atom initially placed above Cu atom 1 is stabilized at the short bridge site between the Cu atoms labeled 1 and 3, resulting in the adsorption energy of 0.47 eV, the adsorption energy for the oxygen atom atop Cu atom 2 is 1.52 eV. Their positive adsorption energies suggest that the extra oxygen atoms cannot be stabilized at the on-surface sites including the short-bridge sites between Cu atoms. This indicates a transition to subsurface oxygen adsorption when the oxygen coverage is greater than 2/3. As shown below, this is indeed the case: the subsurface oxygen adsorption results in a negative value of the adsorption energy.

Table 3
The oxygen adsorption energies for distinct subsurface sites at the oxygen coverage $\theta = 11/12$ (8 on-surface and 3 subsurface oxygen atoms with the Op1 + Op3 configuration).

Adsorption site	Adsorption energy E_{ads}/eV	Stabilized site
Op2	−0.55	
O1	−0.50	T1
O3	−0.53	
O4	−0.28	
O6	−0.58	
T1	−0.50	
T2	−0.53	O3
T3	−0.58	O2
T4	−0.28	

3.1. Oxygen coverage of $\theta = 3/4$

The oxygen coverage of 3/4 is achieved by placing one additional oxygen atom into the subsurface region of the Cu(110)-$c(6 \times 2)$ reconstructed surface. The number of possible adsorption sites examined is greatly reduced by considering the mirror and rotational symmetries of the system. Throughout this study, considerable attention has been paid to ensure that the oxygen adsorption energetics for all non-equivalent subsurface sites are compared. The adsorption energies computed for all the distinct sites are listed in Table 1, and the relaxed structures are shown in Fig. 2. The Op1 configuration gives the most stable structure with the adsorption energy of −0.90 eV. It is interesting to note that after the structural relaxation the Op1 subsurface oxygen atom is bonded with three Cu atoms, two on the second layer and the other Cu atom on the third layer. The bond lengths to the three coordinating Cu atoms are 1.97 Å, 1.97 Å and 1.95 Å, and the Cu–O–Cu bond angles are 82.73°, 85.17° and 85.17°, respectively, suggesting that when the subsurface adsorption initiates, the oxygen atom prefers to stay at a pseudo threefold position above the second layer, which is similar to the on-surface oxygen adsorption on a clean Cu(110) surface, where the oxygen atom stays at a pseudo threefold position above the surface by involving two on-surface Cu atoms and one Cu atom from the second Cu layer [29,31]. The introduction of Op1 oxygen makes no structural change on the top layer, which can be seen in Fig. 2(a), and the top surface has negligible upward relaxation (only ~0.11%) as measured from the average height change between the on-surface oxygen atoms and the first-layer Cu atoms. The most stable octahedral site is found to be O3 (identically, O4, O9 and O10), with the adsorption energy of −0.71 eV, compared with −0.61 eV for O1 site. The preference of O3 over O1 can be attributed to the increased coordinating Cu atoms at O3 site, which is bonded with 6 Cu atoms (two Cu atoms at each of the first three layers), whereas the oxygen at O1 is bonded with five Cu atoms. The formation of Cu–O bonds has been shown effective in bringing down the system energy [31]. The tetrahedral sites yield the highest adsorption energies, indicating that they are the least favorable sites for oxygen subsurface occupancy.

3.2. Oxygen coverage of $\theta = 5/6$

We then add another oxygen atom into various subsurface positions of the most stable Op1 configuration and achieve an oxygen coverage of 5/6 with a total of two subsurface oxygen atoms. The adsorption energies for the nonequivalent positions are listed in Table 2. The open site Op3 is the most stable adsorption position under such an oxygen coverage (note that Op1 is already pre-occupied by oxygen, but it still has freedom to relax its position during the subsequent oxygen adsorption). The preference of Op3 (Fig. 3(b)) site over Op2 (Fig. 3(a)) can be attributed to the fact that the distance between Op1 and Op2 sites is much

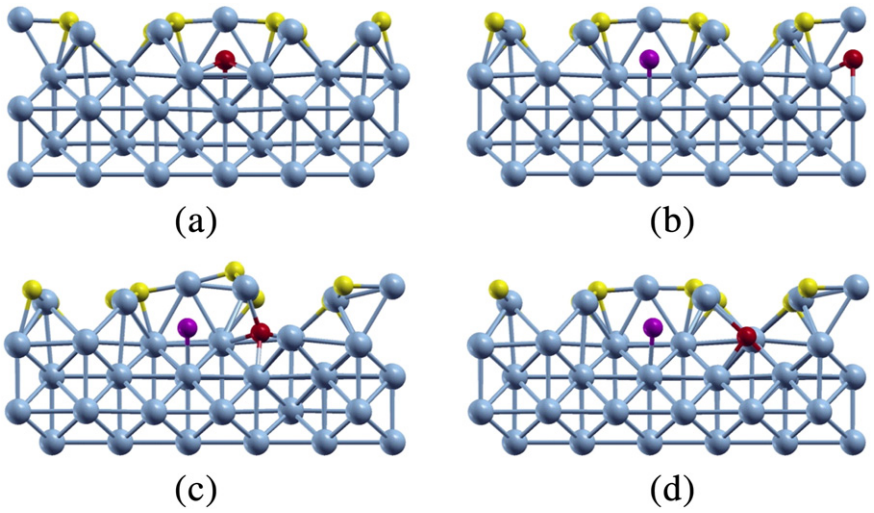

Fig. 3. Relaxed structures of $c(6 \times 2)$ cell at an oxygen coverage of $\theta = 5/6$, with oxygen atoms adsorbed at various subsurface sites: (a) Op2, (b) Op3, (c) the oxygen atom initially placed at O5 moves to T6 and (d) the oxygen atom initially placed at T5 moves to O3. Cu atoms are depicted by blue balls, on-surface oxygen atoms by yellow balls. Red balls represent the newly adsorbed subsurface oxygen atoms, while purple balls represent the old ones (note that only some representative structures are presented while other configurations of less importance are not shown).

smaller than that between Op1 and Op3, resulting in larger repulsion between the oxygen atoms at Op1 and Op2 sites and thus making Op2 less favorable for oxygen to occupy. Our calculation shows that the introduction of Op3 subsurface oxygen leads to minor expansion of the top surface by 0.39% (which is translated into an average height increase of 0.02 Å) compared with the $c(6 \times 2)$ surface with no subsurface oxygen.

Several structural changes are observed after the relaxations. The oxygen atom originally placed at O5 moves to T6 after relaxation (Fig. 3(c)), while the oxygen atoms put at T5 and T8 are finally stabilized at O3 (Fig. 3(d)) and O6, respectively, suggesting that the presence of open-site oxygen atom makes its adjacent octahedral/tetrahedral sites unfavorable for further oxygen adsorption due to repulsive interaction. Although the tetrahedral sites are still not favorable for oxygen adsorption, the most stable tetrahedral site gives an adsorption energy (−0.59 eV at T6) very close to that of the more stable octahedral sites (−0.61 eV at O3 and O6) at this oxygen coverage.

3.3. Oxygen coverage of $\theta = 11/12$

We then add another oxygen atom into the various subsurface positions of the most stable Op1 + Op3 configuration (i.e., these two sites are pre-occupied by oxygen) and achieve the oxygen coverage of $\theta = 11/12$ with the total of three subsurface oxygen atoms. The oxygen adsorption energies for the non-equivalent subsurface sites are listed in Table 3. At this oxygen coverage, the open sites (Fig. 4(a)) no longer yield the lowest system energy, and the adsorption energy of O4 (Fig. 4(c)) is significantly higher than other octahedral sites (i.e., Fig. 4(b) and (d)). O6 turns to be the most stable site for oxygen adsorption, with the adsorption energy of −0.58 eV and a top surface height elevation of 2.35% (Fig. 4(d)) compared with that of the pure $c(6 \times 2)$ surface. Interestingly, the oxygen atom initially placed at the O1 site is stabilized at T1 after structural relaxation, similar as the oxygen atom that is initially placed at O5 but stabilized at T6 at the coverage of 5/6 ML. T1 (Fig. 4(e)) and T4 (Fig. 4(f)) maintain their tetrahedral feature after relaxation, while the oxygen atoms initially placed at T2 and T3 sites move to their adjacent octahedral sites.

3.4. Oxygen coverage of $\theta = 1$

We then add another oxygen atom into the various subsurface positions of the most stable configuration of the Op1 + Op3 + O6. With four subsurface oxygen atoms, the total oxygen coverage reaches 1 ML. The system symmetry is broken by the pre-occupancy of oxygen atoms at Op1, Op3 and O6 sites (note these atoms are still allowed to relax their positions during the subsequent oxygen adsorption), thus the number of nonequivalent subsurface sites increases significantly and we consider oxygen adsorption at all these subsurface sites. The adsorption energies obtained are given in Table 4, and representative relaxed structures are shown in Fig. 5. It can be seen that with the introduction of the fourth subsurface oxygen atom, the previously adsorbed oxygen may move to some other adjacent higher-symmetry sites. For instance, the oxygen atom stabilized at O6 at the oxygen coverage $\theta = 11/12$ now moves to T7 after the fourth oxygen atom is placed at Op2 (Fig. 5(a)), and the oxygen atom that initially resides Op1 moves to O5 after O7 is occupied by a new oxygen atom (Fig. 5(b)). As it happens for the lower coverages, if an open site is already occupied, it becomes energetically unfavorable for other oxygen atoms to take its adjacent octahedral sites: the oxygen atoms initially placed at O1, O5, O8 and O11 are finally stabilized at T1, T6, T11 and T13, respectively (Fig. 5(c–e)). More importantly, oxygen atom that initially resides at O5 moves to T6 after relaxation, resulting in the most stable configuration at 1 ML coverage and ~4.67% of the top surface height elevation. However, it is noted that many of the tetrahedral sites are still not stable oxygen residence sites, and oxygen atoms originally put into these positions are finally found at the nearby octahedral sites, as listed in

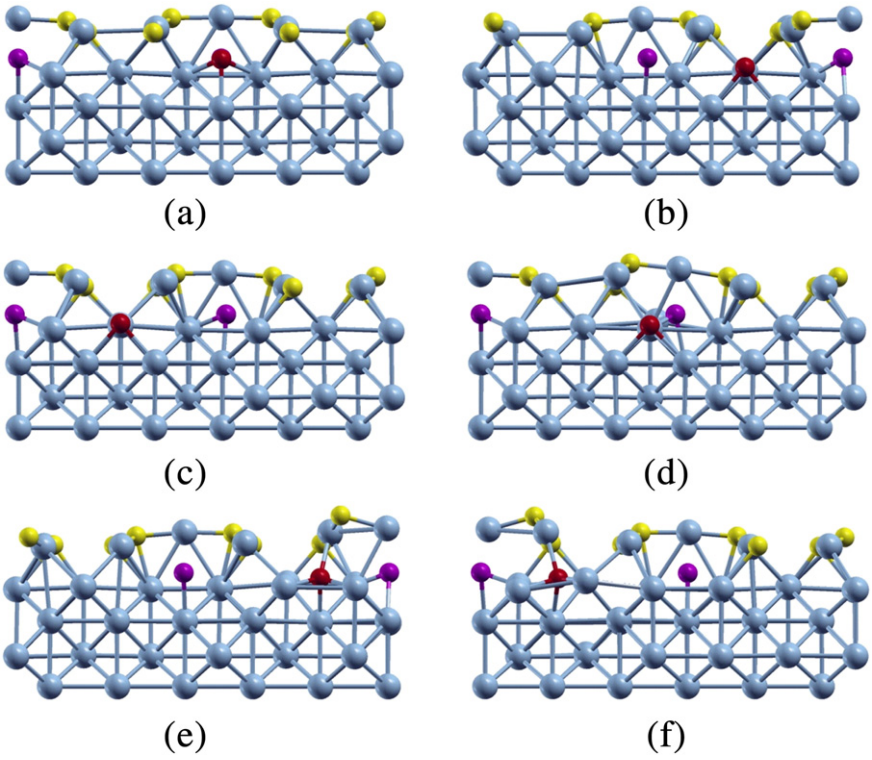

Fig. 4. Relaxed structures of $c(6 \times 2)$ cell at an oxygen coverage of $\theta = 11/12$, with oxygen atoms adsorbed at various subsurface sites: (a) Op2, (b) O3, (c) O4, (d) O6, (e) T1 and (f) T4. Cu atoms are depicted by blue balls, on-surface oxygen atoms by yellow balls. Red balls represent the newly adsorbed subsurface oxygen atoms, and purple balls are for old ones.

Table 4
The adsorption energies of the subsurface oxygen atoms at the oxygen coverage $\theta = 1$ (8 on-surface and 4 subsurface oxygen atoms with the Op1 + Op3 + O6 configuration).

Adsorption site	Adsorption energy E_{ads}/eV	Stabilized site
Op2	−0.69	O6 moves to T7
Op4	−0.56	
O1	−0.41	T1
O2	−0.68	
O3	−0.59	
O4	−0.63	
O5	−0.71	T6
O7	−0.20	Op1 moves to O5
O8	−0.53	T11
O9	−0.55	
O10	−0.43	
O11	−0.59	T13
O12	−0.60	
T1	−0.41	
T2	−0.59	O3
T3	−0.66	
T4	−0.63	
T5	−0.58	O3
T6	−0.71	
T7	−0.49	
T8	−0.15	
T9	−0.55	O9
T10	−0.39	
T11	−0.53	
T12	−0.43	O10
T13	−0.59	
T14	−0.55	O9
T15	−0.60	O12
T16	−0.46	

Table 4. Fig. 5(f) shows the relaxed configuration for which the oxygen atom is initially placed at T2 but finally stabilized at O3. It is worth to point out that the second most stable configuration, which is obtained by initially positioning one oxygen atom into the Op2 site, is also a tetrahedral-site oxygen atom stabilized at the T7 site.

4. Discussion

By looking at the adsorption energies at distinct subsurface sites for the different oxygen coverages, we find that there is an increasing tendency for the newly adsorbed oxygen atom to stabilize at the tetrahedral site with increasing the oxygen coverage. Such a transition to the oxygen tetrahedral preference can be attributed to the upward relaxation of the top surface layer with the increased oxygen coverage, which makes room available for oxygen tetrahedral occupancy. The top surface layer relaxes upward as the subsurface oxygen coverage increases and thus induces larger interplanar space between the first and second layer for tetrahedral oxygen occupancy. From Figs. 2(a) and 3(b), it can be seen that the embedment of subsurface oxygen atoms at Op1 and Op3 sites causes negligible surface elevation, and the top surface morphology remains unchanged compared with that of the pure $c(6 \times 2)$ structure. However, further oxygen adsorption induces pronounced upward surface relaxation, which makes it possible for oxygen atoms to reside tetrahedral sites. On the other hand, it can be also noted that at the oxygen coverages less than 1 ML the oxygen adsorption energies increase as more subsurface oxygen atoms are adsorbed into the open or octahedral sites. However, once the oxygen coverage $\theta = 1$ is reached, oxygen atom begins to reside tetrahedral sites and the adsorption energy for the most stable configuration decreases pronouncedly (from −0.58 eV to −0.71 eV

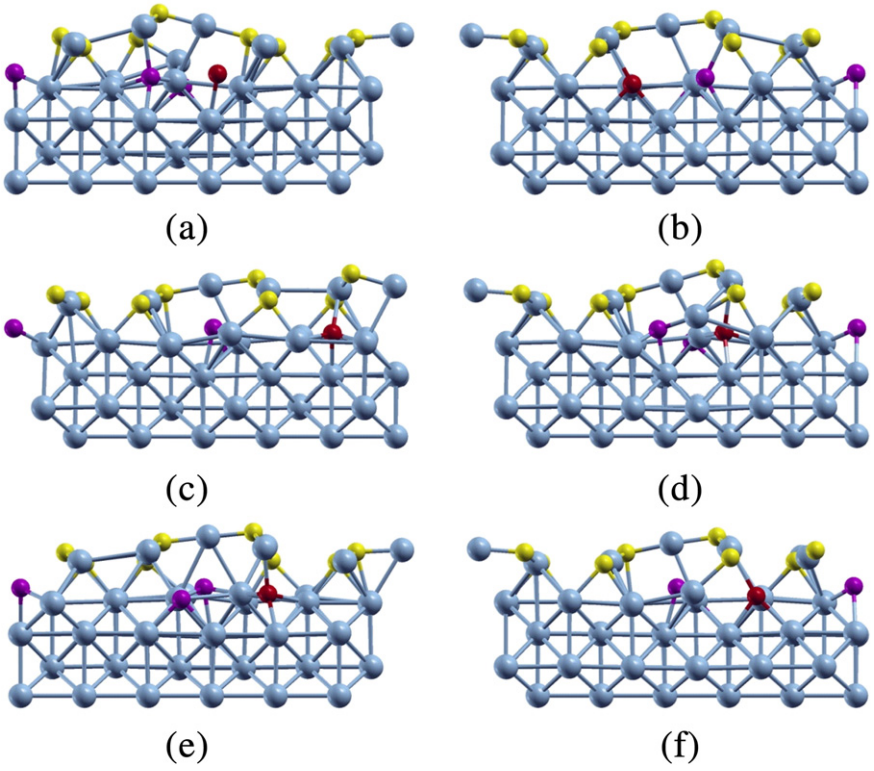

Fig. 5. Relaxed structures of $c(6 \times 2)$ cell at an oxygen coverage of $\theta = 1$, with oxygen atoms adsorbed at various subsurface sites: (a) Op2, making the pre-adsorbed oxygen at O6 move to T7, (b) O7, making the pre-adsorbed oxygen at Op1 move to O5, (c) the oxygen atom placed at O1 moves to T1, (d) the oxygen atom initially placed at O5 moves to T6, (e) the oxygen atom initially placed at O8 moves to T11 and (f) the oxygen atom initially placed at T2 moves to O3. Cu atoms are depicted by blue balls, on-surface oxygen atoms by yellow balls. Red balls represent the newly adsorbed subsurface oxygen atoms, and purple balls are for old ones.

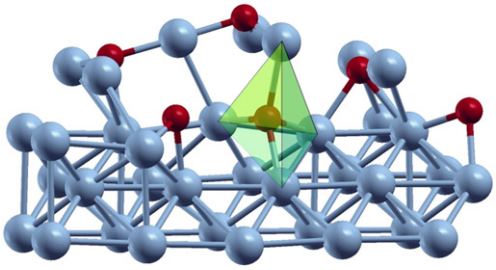

Fig. 6. Equilibrium structure of the tetrahedron formed from the oxygen subsurface adsorption at T6 for the oxygen coverage $\theta = 1$. The resulting Cu_2O-like tetrahedron is highlighted, in which Cu atoms are depicted by blue balls and O atoms by red balls.

by comparing the energies listed in Tables 3 and 4), revealing that the tetrahedral adsorption contributes to the system stability.

We now examine the atomic structure of the tetrahedron resulted from the most stable configuration at the 1 ML oxygen coverage since the oxygen tetrahedral adsorption may indicate the onset of the bulk oxide (Cu_2O) formation. Fig. 6 shows the resulting tetrahedron at T6 for the 1 ML oxygen coverage. Our measurement shows that the Cu – O bond lengths of the tetrahedron ranges from 1.89 Å to 2.09 Å, and the Cu – O – Cu bond angles fall into the range of 87.23° to 139.62°. According to our DFT calculation, the corresponding bond length and bond angle in bulk Cu_2O are 1.86 Å and 109.47°, respectively. It is clear that the tetrahedral structure formed at T6 shows some distortion compared with a perfect Cu_2O tetrahedron.

Our results demonstrate that the tetrahedral preference occurs at the $c(6 \times 2)$ reconstructed Cu(110) surface with 1 ML oxygen coverage. This is in contrast to the Cu(100) surface, for which the oxygen tetrahedral preference was observed only under some special conditions. The oxygen tetrahedral preference over octahedral sites occurs when the oxygen coverage reaches 0.75 ML by assuming a nonreconstructed Cu(100) surface [14,47]. Realistically, a missing-row surface reconstruction has already taken place that has a saturated oxygen coverage of 0.5 ML [48–52]. For the missing-row reconstructed Cu(100) surface, Lee et al. noted that the oxygen tetrahedral adsorption can occur at the oxygen coverage of 1 ML with the presence of an oxygen molecule adsorbed on the reconstructed Cu(100) surface; if the oxygen molecule is absent, no tetrahedral adsorption occurs even under a higher oxygen coverage [17]. More recently, we found that the oxygen tetrahedral adsorption at a lower oxygen coverage of 0.53 ML can also occur only along the defect area (i.e., domain boundaries) formed by merging missing-row domains [19]. However, for the $c(6 \times 2)$ reconstructed Cu(110) surface, we monitor the oxygen adsorption process with increasing the oxygen coverage and obtain the oxygen tetrahedral preference at the oxygen coverage of 1 ML without involving any defect areas or molecular oxygen adsorbed on the surface. These differences suggest that the Cu(110) surface has a stronger tendency to form Cu_2O-like tetrahedrons than Cu(100) with increasing the atomic oxygen coverage. This corroborates with a previous *in situ* electron microscopy study that showed that the Cu(110) surface has a faster initial oxidation kinetics (i.e., the nucleation and growth rates of Cu_2O nanoislands) than Cu(100) [53].

The differences between Cu(100) and Cu(110) in the transition from oxygen octahedral adsorption to tetrahedral adsorption may be related to the numbers of octahedral and tetrahedral sites available for oxygen subsurface adsorption. Fig. 7 shows the missing-row reconstructed Cu(100) unit cell from which we can determine the number of subsurface octahedral and tetrahedral adsorption sites (note that both fully and under-coordinated octahedral and tetrahedral sites are accounted). The positions of the octahedral/tetrahedral sites at the Cu(110)-$c(6 \times 2)$ reconstructed surface can be seen in Fig. 1(b) and (c), respectively. Both the (100) and (110) surface reconstructions shown in Figs. 7 and 1 correspond to the highest oxygen coverages before oxygen subsurface adsorption takes place. For the missing-row reconstructed Cu(100) surface, the densities of subsurface octahedral and tetrahedral adsorption sites are $0.15/Å^2$ and $0.30/Å^2$, respectively, while for the $c(6 \times 2)$ reconstruction, their densities are $0.11/Å^2$ and $0.14/Å^2$, respectively. Apparently, the Cu(110)-$c(6 \times 2)$ surface has less octahedral sites, which may drive the transition to the oxygen tetrahedron occupancy at a lower oxygen coverage compared to the Cu(100) surface. Such a crossover may be linked with the onset of the bulk oxide formation.

5. Conclusion

Using DFT method, we extensively studied the stability and structural change of Cu(110)-$c(6 \times 2)$ surface under the increased the oxygen coverage. As the surface oxygen coverage goes up, oxygen subsurface adsorption occurs, which induces the elevation of the top surface layer. It is found that the oxygen can be stabilized at the tetrahedral site when the coverage reaches 1 ML, which demonstrates that a critical oxygen coverage exists for the occurrence of tetrahedral preference. The crossover from oxygen octahedral adsorption to tetrahedral adsorption may signal the onset of bulk oxide formation. The bond lengths and bond angles of the resulting Cu – O tetrahedron formed at the 1 ML oxygen coverage show some distortion compared with that of the bulk Cu_2O phase. A comparison with the oxygen adsorption at Cu(100) suggest that the Cu(110) surface has a larger tendency to form Cu – O tetrahedrons.

Acknowledgment

Research supported by the U.S. Department of Energy, Office of Basic Energy Sciences, Division of Materials Sciences and Engineering under Award No. DE-FG02-09ER46600. This work used the computational resources from the Extreme Science and Engineering Discovery

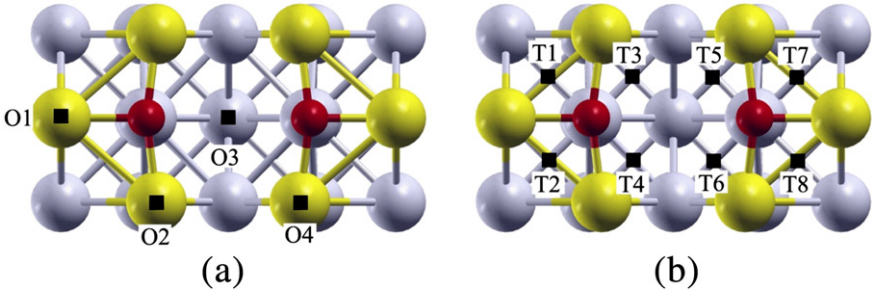

Fig. 7. The structure models of the missing-row reconstructed Cu(100) surface, where the subsurface interstitial sites are highlighted. (a) 4 octahedral sites, (b) 8 tetrahedral sites. The first Cu layer is depicted by yellow balls, second-fifth Cu layers by gray balls and on-surface O atoms by red balls.

Environment (XSEDE) provided by SDSC Trestles, which is supported by National Science Foundation grant number OCI-1053575.

Appendix A. Supplementary data

Supplementary data to this article can be found online at http://dx.doi.org/10.1016/j.susc.2013.04.005.

References

[1] T. Huang, D. Tsai, Catal. Lett. 87 (2003) 173.
[2] F. Jing, Y. Zhang, S. Luo, W. Chu, H. Zhang, X. Shi, J. Chem. Sci. 122 (2010) 621.
[3] B. White, M. Yin, A. Hall, D. Le, S. Stolbov, T. Rahman, N. Turro, S. O'Brien, Nano Lett. 6 (2006) 2095.
[4] H. Over, Y.D. Kim, A.P. Seitsonen, S. Wendt, E. Lundgren, M. Schmid, P. Varga, A. Morgante, G. Ertl, Science 287 (2000) 1474.
[5] C. Stampfl, M.V. Ganduglia-Pirovano, K. Reuter, M. Scheffler, Surf. Sci. 500 (2002) 368.
[6] S. Mrowec, Corros. Sci. 7 (1967) 563.
[7] R.A. Rapp, Metall. Trans. A 15 (1984) 765.
[8] Y. Lee, W. Tsai, J. Maa, Appl. Surf. Sci. 173 (2001) 352.
[9] H. Zhang, Q. Zhu, Y. Zhang, Y. Wang, L. Zhao, B. Yu, Adv. Funct. Mater. 17 (2007) 2766.
[10] X. Gou, G. Wang, J. Yang, J. Park, D. Wexler, J. Mater. Chem. 18 (2008) 965.
[11] K. Nomura, H. Ohta, A. Takagi, T. Kamiya, M. Hirano, H. Hosono, Nature 432 (2004) 488.
[12] A. Gupta, A.D. Compaan, Appl. Phys. Lett. 85 (2004) 684.
[13] S. Jeong, Y.G. Ha, J. Moon, A. Facchetti, T.J. Marks, Adv. Mater. 22 (2010) 1346.
[14] T. Kangas, K. Laasonen, A. Puisto, H. Pitkänen, M. Alatalo, Surf. Sci. 584 (2005) 62.
[15] T. Kangas, K. Laasonen, Surf. Sci. 602 (2008) 3239.
[16] M. Lee, A.J.H. McGaughey, Surf. Sci. 603 (2009) 3404.
[17] M. Lee, A.J.H. McGaughey, Surf. Sci. 604 (2010) 1425.
[18] B. Jeon, S.K.R.S. Sankaranarayanan, A.C.T. van Duin, S. Ramanathan, Philos. Mag. 91 (2011) 4073.
[19] L. Li, X. Mi, Y. Shi, G. Zhou, Phys. Rev. Lett. 108 (2012) 176101.
[20] W.A. Saidi, M. Lee, L. Li, G. Zhou, A.J.H. McGaughey, Phys. Rev. B 86 (2012) 245429.
[21] G. Ertl, Surf. Sci. 6 (1967) 208.
[22] R. Feidenhans'l, I. Stensgaard, Surf. Sci. 133 (1983) 453.
[23] D.J. Coulman, J. Wintterlin, R.J. Behm, G. Ertl, Phys. Rev. Lett. 64 (1990) 1761.
[24] F. Jensen, F. Besenbacher, E. Laegsgaard, I. Stensgaard, Phys. Rev. B 41 (1990) 10233.
[25] K.W. Jacobsen, J.K. Nørskov, Phys. Rev. Lett. 65 (1990) 1788.
[26] R. Feidenhans'l, F. Grey, M. Nielsen, F. Besenbacher, F. Jensen, E. Laegsgaard, I. Stensgaard, K.W. Jacobsen, J.K. Nørskov, R.L. Johnson, Phys. Rev. Lett. 65 (1990) 2027.
[27] B.G. Briner, M. Doering, H.-P. Rust, A.M. Bradshaw, Phys. Rev. Lett. 78 (1997) 1516.
[28] F. Frechard, R.A. van Santen, Surf. Sci. 407 (1998) 200.
[29] S.Y. Liem, G. Kresse, J.H.R. Clarke, Surf. Sci. 415 (1998) 194.
[30] S.Y. Liem, J.H.R. Clarke, G. Kresse, Surf. Sci. 459 (2000) 104.
[31] X. Duan, O. Warschkow, A. Soon, B. Delley, C. Stampfl, Phys. Rev. B 81 (2010) 075430.
[32] C. Poulain, F. Wiame, V. Maurice, P. Marcus, Surf. Sci. 606 (2012) L26.
[33] G. Kresse, J. Hafner, Phys. Rev. B 47 (1993) 558.
[34] G. Kresse, J. Hafner, Phys. Rev. B 49 (1994) 14251.
[35] G. Kresse, J. Furthmüller, Comput. Mater. Sci. 6 (1996) 15.
[36] G. Kresse, J. Furthmüller, Phys. Rev. B 54 (1996) 11169.
[37] J.P. Perdew, K.A. Jackson, M.R. Pederson, D.J. Singh, C. Fiolhais, Phys. Rev. B 46 (1992) 6671.
[38] G. Kresse, D. Joubert, Phys. Rev. B 59 (1999) 1758.
[39] P.E. Blöchl, Phys. Rev. B 50 (1994) 17953.
[40] G. Zhou, L. Luo, L. Li, J. Ciston, E. Stach, J.C. Yang, Phys. Rev. Lett. 109 (2012) 235502.
[41] H.J. Monkhorst, J.D. Pack, Phys. Rev. B 13 (1976) 5188.
[42] M. Methfessel, A. Paxton, Phys. Rev. B 40 (1989) 3616.
[43] A. Kokalj, Comput. Mater. Sci. 28 (2003) 155.
[44] G. Herzberg, Can. J. Phys. 30 (1952) 185.
[45] B. Hammer, L. Hansen, J. Nørskov, Phys. Rev. B 59 (1999) 7413.
[46] J.P. Perdew, K. Burke, M. Ernzerhof, Phys. Rev. Lett. 77 (1996) 3865.
[47] M. Lee, A.J.H. McGaughey, Phys. Rev. B 83 (2011) 165447.
[48] F. Leibsle, Surf. Sci. 337 (1995) 51.
[49] F. Jensen, F. Besenbacher, E. Laegsgaard, I. Stensgaard, Phys. Rev. B 42 (1990) 9206.
[50] H. Iddir, D. Fong, P. Zapol, P. Fuoss, L. Curtiss, G. Zhou, J. Eastman, Phys. Rev. B 76 (2007) 241404.
[51] M. Lampimäki, K. Lahtonen, M. Hirsimäki, M. Valden, J. Chem. Phys. 126 (2007) 034703.
[52] K. Lahtonen, M. Hirsimäki, M. Lampimäki, M. Valden, J. Chem. Phys. 129 (2008) 124703.
[53] G. Zhou, J.C. Yang, Surf. Sci. 531 (2003) 359.